CrystEngComm

Cite this: *CrystEngComm*, 2012, **14**, 2669

www.rsc.org/crystengcomm

PAPER

Self-assembled porous hierarchical-like CoO@C microsheets transformed from inorganic–organic precursors and their lithium-ion battery application†

Jun Liu,[a] Yichun Zhou,*[a] Chunping Liu,[a] Jinbin Wang,[a] Yong Pan[a] and Dongfeng Xue*[bc]

Received 8th November 2011, Accepted 3rd January 2012
DOI: 10.1039/c2ce06497a

Self-assembled porous hierarchical-like CoO@C nanoarchitectures have been fabricated on a large scale through a facile solution-phase process and subsequent annealing of the inorganic–organic $Co(OH)_2$–DS (dodecyl sulphate) precursor nanocomposites. The as-formed porous hierarchical-like CoO@C nanohybrid as an anode material for lithium-ion batteries can exhibit not only a highly reversible capacity but also excellent cycling performance as well as good rate capability. Results show that these hierarchical microsheets made of interconnected CoO tiny nanoparticles are uniformly encapsulated within two-dimensional thin carbon layers. The synergistic effect of both the hierarchical nanoarchitecture and conducting carbon layer support contributes to the enhanced electrochemical performances of the hybrid CoO@C electrode. Importantly, the process to fabricate such a hierarchical nanostructure is facile, low-cost, and scalable, providing a universal approach for the rational design and engineering of self-assembled hierarchical-like electrode materials with enhanced performance, which may have utilities in other applications such as catalysis and sensors.

1. Introductions

Lithium-ion batteries, as energy storage devices dominating power sources for portable electronics and electrical/hybrid vehicles, have been attracting considerable attention in scientific and industrial communities.[1,2] The ever-growing market demand for their high electromotive force, high energy density, and high cyclability has stimulated numerous research efforts aimed at the development of new high performance electrode materials for lithium-ion batteries.[3–7] For example, transition metal oxides including Fe_2O_3, Fe_3O_4 and Co_3O_4 are capable of Li^+ insertion/extraction in excess of 6 Li per formula unit,[8–10] which have attracted a lot of interest when recently used as anode materials for lithium-ion batteries due to their higher theoretical capacities than that of commercial graphite. However, an intrinsically induced drastic volume change gives rise to pulverization that may block the electrical contact pathways in general metal-oxide anodes, thus leading to dramatic decay in capacity and limiting their practical application.[4] Therefore, developing new synthetic strategies to synthesize high-performance metal-oxide electrode materials with large reversible capacity, high cyclability and rate capability still remains a great challenge to chemists and materials scientists.

Constructing nanostructured electrode materials can enhance the electrochemical performances that could not be achieved in bulk materials, benefiting from the large surface area and short diffusion path in nanostructured electrode materials.[4–7] In particular self-assembled hierarchical-like nanostructured inorganic materials attract much attention in a variety of fields because of their extraordinarily high active surface/interface and robust stability.[5,6,11,12] Electrode materials with a hierarchical nanoarchitecture can exhibit intriguing properties by taking advantage of both nanoscale effect and high stability of the secondary-structure assemblies.[4,13] Furthermore, coating active electrode materials with conductive carbon which exhibits superior electrical conductivity and chemical stability has been widely adopted to prevent the exfoliation of active materials and improve the electrical conductivity of electrode materials.[13,14] The thin carbon layer can provide a support for loading electrode nanoparticles and act as a highly conductive matrix for good contact between them.[15] More importantly, thin carbon layers prevent the volume expansion/contraction and the aggregation of electrode nanoparticles effectively during charge/discharge processes.[16] In this regard, both specific capacity and cycling performance of oxide-based nanocomposites can be improved effectively.

Since the discovery of the reversible conversion mechanism of lithium storage was evidently demonstrated, cobalt oxides

[a]*Key Laboratory of Low Dimensional Materials & Application Technology, Ministry of Education, Faculty of Materials, Optoelectronics and Physics, Xiangtan University, 411105, China. E-mail: zhouyc@xtu.edu.cn; Fax: (+) 86-731-58293586; Tel: (+) 86-731-58298119*
[b]*School of Chemical Engineering, Dalian University of Technology, Dalian, 116024, China*
[c]*State Key Laboratory of Rare Earth Resource Utilization, Changchun Institute of Applied Chemistry, Chinese Academy of Sciences, Changchun, 130022, China. E-mail: dongfeng@ciac.jl.cn*
† Electronic supplementary information (ESI) available: other characterizations of precursors and products. See DOI: 10.1039/c2ce06497a

(Co_3O_4 and CoO) have long been promising alternative anode materials to graphite, which have a higher theoretical specific capacity.[3,4] It is reported that nanostructured cobalt oxide-based materials hold the promise of an enhanced capacity higher than that of their bulk counterparts.[17–22] A number of research activities have been reported about nanostructured cobalt oxide anodes including nanotubes, nanowires, nanobelts, nanocapsules and nanocomposites.[17–22] To meet the ever-increasing nanotechnological and energy demand, the diversity of desired nanoarchitectures for high-capacity and long-lifetime CoO-based anode materials still needs to be greatly expanded. Despite the urgent appeal of this kind of porous nanocomposites, there are few well established facile and scalable methods to synthesize these advanced nanostructured composites. Usually, the multi-step coating, currently used for this kind of nanocomposite electrode is time-consuming and tedious, which significantly hinders the process scale-up.[23] Herein, we reported the large-scale fabrication of self-assembled porous hierarchical-like CoO@C nanoarchitectures through a facile solution-based method combined with a subsequent annealing process. It is found that the as-obtained CoO@C nanohybrid comprises both the hierarchical CoO nanostructures and the conducting thin carbon layers. When used as anode materials, they exhibit highly reversible capacity, excellent cyclic performance and good rate capability.

2. Experimental section

Preparation of self-assembled porous hierarchical-like CoO@C microsheets

All the reagents used in the experiments were of analytical grade (Shanghai Chemical Reagent Company) and used without further purification. In a typical synthesis process of this kind of nanocomposites, 2 mmol $Co(NO_3)_2 \cdot 6H_2O$ and 1 mmol sodium dodecyl sulfate (SDS) were dissolved in 20–40 mL mixture of absolute ethanol and distilled water, and stirred for about 1 h. After a clear transparent solution was formed, the mixture was then transferred into a 30–50 mL Teflon-lined stainless steel autoclave, which was sealed and maintained at 180 °C for 24 h. The as-synthesized sample was further annealed at 550 °C in a N_2 flow to obtain the final product of hierarchical-like CoO@C microsheets constructed with nanosheets. Bare CoO microsheets were prepared by the similar reaction routes, but in the absence of structure-directing agent SDS.

Materials characterization

The collected products were characterized by an X-ray diffractometry (XRD) on a Rigaku-DMax 2400 diffractometer equipped with the graphite monochromatized Cu-Kα radiation flux at a scanning rate of 0.02° s^{-1}. The microstructure of samples was investigated by means of scanning electron microscopy (SEM, JEOL-5600LV) and transmission electron microscopy (TEM, Philips, TecnaiG2 20). Energy-dispersive X-ray spectroscopy (EDS) microanalysis of these samples was performed during SEM measurements. The Fourier transform infrared (FTIR) spectrum of $Co(OH)_2$–DS were recorded on a Perkin-Elmer Spectrum One FTIR Spectrometer. The N_2 adsorption/desorption isotherm was obtained at 77 K using Beishide Instrument-ST, 3*H*-2000PS2. The BET surface area was estimated using adsorption data in a relative pressure ranging from 0.05 to 0.3.

Electrochemical measurements

The electrochemical performances of the as-prepared products were measured by using CR2025 coin cells at 0.01–3.00V with NEWARE-BTS-5V20mA battery test system. For the preparation of the working electrode, a mixture of CoO@C active material, carbon black, and polyvinylidene fluoride (PVDF) in the weight ratio of 80 : 15 : 5 was ground in a mortar with *N*-methy1-2-pyrrolidone (NMP) as solvent to make slurry. A Li foil was used as the counter electrode and a solution of 1M $LiPF_6$ in ethylene carbonate (EC)/diethyl carbonate (DEC) (1 : 1 in volume) was used as electrolyte.

3. Results and discussion

The inorganic–organic layered precursors were synthesized *via* a simple, effective coprecipitation method using sodium dodecyl sulfate (SDS) as the structure-directing agent. Fig. 1 illustrates the use of this one-step hydrothermal crystallization process to prepare $Co(OH)_2$ nanosheet-based hierarchical microsheets, which can be converted into self-assembled porous hierarchical-like CoO@C microsheets. The homogeneous precipitation method of $Co(NO)_3$ hydrolysis in water/alcohol mixture was used to form a $Co(OH)_2$ intercalated with dodecyl sulphate ($Co(OH)_2$–DS). During the hydrothermal crystallization process, these newly formed $Co(OH)_2$–DS nanosheets can self-assemble *via* layer-by-layer, forming hierarchical microsheets. Then, the resulting inorganic–organic nanocomposites were further annealed at 550 °C in a N_2 atmosphere, and hierarchical CoO@C nanoarchitectures were finally achieved. The as-obtained CoO component was converted from $Co(OH)_2$ decomposition, while conductive carbon layers were converted from DS carbonization.

Fig. 2a shows the Fourier transform infrared (FTIR) spectra of layered $Co(OH)_2$ intercalated with organic DS anions. The peak at 3600 cm^{-1} was assigned to a νO–H stretching band, and confirmed the presence of a hydroxyl group of the layer structured $Co(OH)_2$.[24] The broad band around 1640 cm^{-1} was

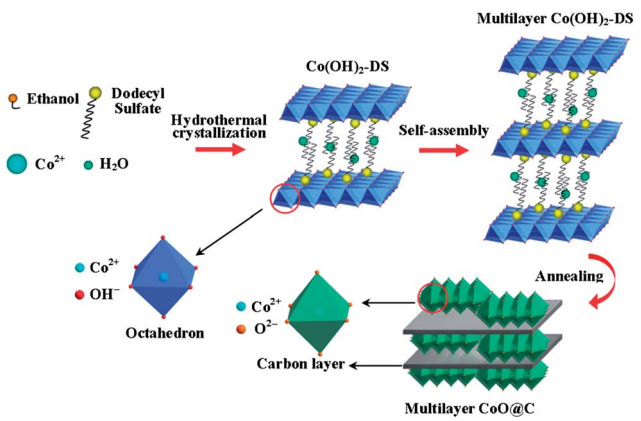

Fig. 1 Schematic illustration of the formation mechanism of self-assembled porous hierarchical-like CoO@C microsheets constructed from nanosheets.

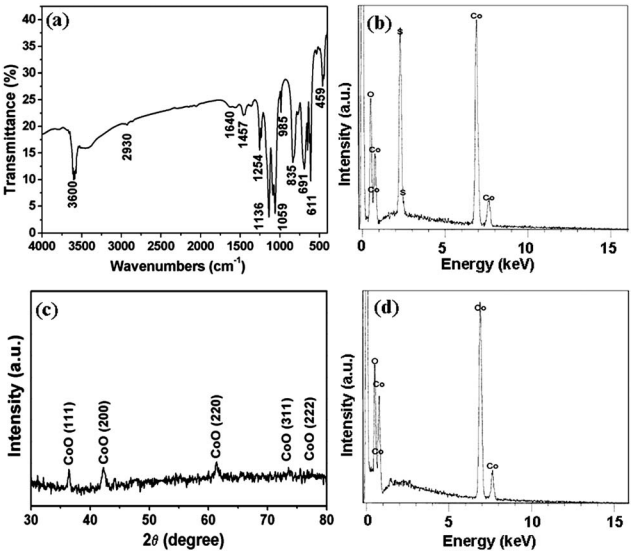

Fig. 2 (a) FTIR spectrum of self-assembled hierarchical-like $Co(OH)_2$–DS inorganic–organic microsheets; (b) EDS spectrum of these inorganic–organic precursor microsheets; (c) XRD patterns of finally self-assembled porous hierarchical-like CoO@C microsheets obtained *via* annealing in N_2 atmosphere; (d) EDS spectrum of these CoO@C products. In Fig. 2b and d, H and C elements were not detected due to the limited sensitivity of EDS microanalysis.

assigned to the $\delta(H_2O)$ vibration of water molecules existing between $Co(OH)_2$ layers.[25] The peak at about 611 cm^{-1} was assigned to the δO–H.[26] Distinct absorptions were present due to C–H stretching vibrations of the alkyl chains of the DS anions at 1457 and 2930 cm^{-1}.[25] The vibration bands at 1136, 1059, 985 and 835 cm^{-1} were observed and assigned to the vibration of SO_4^{2-}.[27,28] The broad absorption at low-frequency region (400–600 cm^{-1}) is ascribed to Co–O stretching and Co–OH bending vibrations in the brucite-like octahedral sheet.[29] It can be evidenced as well by the presence of DS anions between $Co(OH)_2$ layers. Energy-dispersive X-ray spectroscopy (EDS) of these inorganic–organic precursors is shown in Fig. 2b, which also confirms that DS anions have been intercalated into the $Co(OH)_2$ layers. The self-assembled hierarchical-like $Co(OH)_2$–DS microsheets were converted to CoO@C materials after simple calcination in N_2. As shown in Fig. 2c, all the diffraction peaks can be indexed to the standard raw salt cubic CoO, with the lattice constant $a = 4.261$ Å, which is consistent with the value in the standard card (JCPDS card no. 48–1719). No other peaks of impurities are observed. We have calculated the average particle size (D) by X-ray diffractometry (XRD) using the Scherrer equation:

$$D = \frac{0.9\lambda}{\beta \cos\theta} \quad (1)$$

Where D is the crystallite size, λ is the X-ray wavelength, β is the full width at half maximum (FWHM) of the diffraction peak, and θ is the Bragg diffraction angle of the diffraction peaks.[30] The average particle size was found to be 53.3 nm, which is consistent with the TEM characterization. EDS microanalysis (Fig. 2d) clearly confirmed that organic DS anions have been completely converted into inorganic carbon layers, which is consistent with the XRD results (Fig. 2c). The conducting carbon layers were also confirmed by the thermogravimetric analysis (TGA) of these CoO@C microsheets in air (Fig. S3, ESI†), which shows a total weight of 14.7% carbon content.

The morphology and size of these products are further examined by scanning electron microscopy (SEM). Fig. 3 and Fig. 4 show SEM images of these inorganic–organic precursors and finally self-assembled hierarchical CoO@C nanoarchitectures, respectively. Fig. 3a and b show that these precursors consist of relatively uniform hexagonal microsheets with size of 10–15 μm. This hierarchical structure is composed of densely packed layers of hexagonal nanosheets with thickness of 50–100 nm. The formation of such self-assembled hierarchical-like $Co(OH)_2$–DS has been further confirmed by high-magnification image. It is interesting that there is a small hole on the centre of each microsheet (Fig. 3c). Moreover, the close examination of the rims of microsheets reveals a layer-by-layer growth style (Fig. 3d). After calcination in N_2 atmosphere, these self-assembled hierarchical-like nanostructures of $Co(OH)_2$–DS microsheets were converted into CoO@C products. There was no substantial morphology change during this process. As shown in the SEM images (Fig. 4), the hierarchical-like microsheets, consisting of a large quantity of CoO@C nanosheets, were still observed. Compared to the previous precursor composites, these obtained CoO@C microsheets became largely porous, which were composed of numerous connected small nanoparticles. The calcination temperature has an important effect on the microstructure and composition of the final products during the annealing process. When the calcination temperature is below 550 °C, for example, at 450 °C the inorganic–organic $Co(OH)_2$–DS precursors were not completely converted into inorganic CoO@C products, and partial organic DS were residual, which can degrade the electrochemical performance of the final electrode materials. However, when the calcination temperature is too high, such as at 700 °C partial hierarchical-like CoO@C

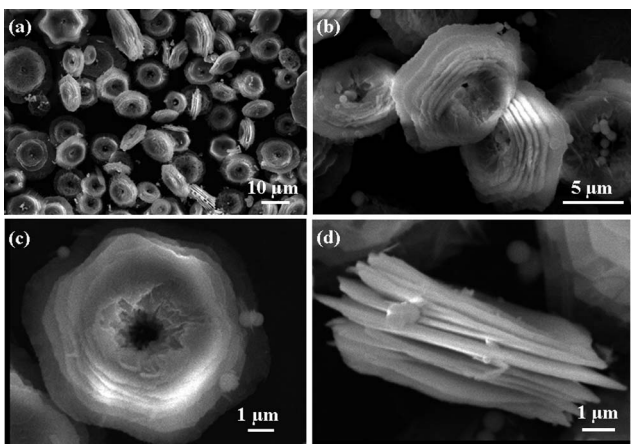

Fig. 3 SEM images of self-assembled hierarchical-like $Co(OH)_2$–DS inorganic–organic microsheets *via* hydrothermal crystallization: (a,b) low-magnification SEM images show that these hierarchical microsheets have a uniform hexagonal morphology and each microsheet has a small hole in the centre; (c) high-magnification SEM image of a typical microsheet showing its surface morphology; (d) high-magnification SEM image of the rim of a hierarchical microsheet revealing densely packed layers of nanosheets.

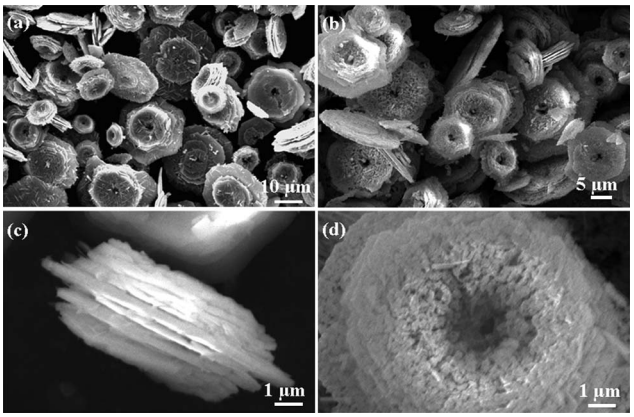

Fig. 4 Different magnification SEM images of finally self-assembled porous hierarchical-like CoO@C microsheets obtained *via* annealing in N_2 atmosphere. All these SEM images clearly show that the as-obtained CoO@C products preserve their $Co(OH)_2$–DS precursor morphology.

microsheets collapsed during the chemical transformation process (Fig. S5, ESI†).

The highly porous characteristic of these CoO@C nanocomposites was further confirmed by transmission electron microscopy (TEM) characterizations. Fig. 5a shows low-magnification TEM image of a typical CoO@C nanosheet, which demonstrates that densely macropores distribute on the surface. The formation of these macropores is ascribe to dehydration and decomposition of $Co(OH)_2$ and DS anions during annealing in N_2 atmosphere.[7] High-magnification TEM images (Fig. 5b and c) exhibit that these macroporous nanosheet were composed of

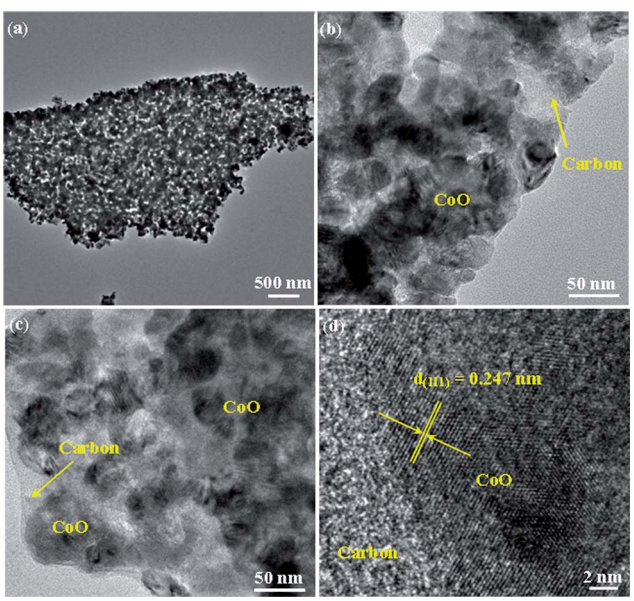

Fig. 5 TEM characterizations of the porous CoO@C nanosheet secondary building blocks which constructed the self-assembled multi-layer CoO@C: (a) low-magnification TEM image of a broken CoO@C nanosheet; (b,c) high-magnification TEM images which clearly show that CoO nanoparticle are homogeneously loaded and encapsulated by thin carbon layers; (d) HRTEM image revealing lattice planes of CoO nanoparticles and the amorphous carbon layer.

numerous connected small nanoparticle, which were encapsulated fully with thin carbon layers. The selected area electron diffraction (SAED) patterns show continuous ring patterns without any rings of secondary phases revealing their polycrystalline structure (Fig. S6, ESI†). A high resolution TEM (HRTEM) image (Fig. 5d) reveals a lattice plane with the interplanar distance of 0.247 nm of these connected small nanoparticles, corresponding to the (111) plane of the CoO cubic crystalline structure.

The surface area of these self-assembled porous hierarchical-like CoO@C microsheets were measured using the Brunauer–Emmett–Teller (BET) method. Fig. 6a and b show the N_2 adsorption–desorption isotherm at 77 K and the pore size distribution by the Barrett–Joyner–Halenda (BJH) method, respectively. The isotherm can be classified a typical III isotherm without a distinct hysteresis loop, which suggests the absence of a distinct mesoporous structure and a BET specific surface area of 9.64 $m^2\ g^{-1}$. The shape of the pore size distribution curve indicates that these hierarchical-like CoO@C microsheets are porous materials and display a broad pore size distribution in the range 25–75 nm. These results are in good agreement with the SEM and TEM images.

Fig. 7a and b show voltage–capacity curves of porous hierarchical-like CoO@C and CoO microsheets at 0.2 C rate (5 h per half cycle, 140 mA g^{-1}), respectively. It is striking to note that a high reversible capacity of about 990 mA h g^{-1} was achieved after 30 cycles (Fig. 7a). For comparison, we fabricated a bare CoO microsheet anode and the bare CoO showed only 51% retention of the initial reversible capacity after 20 cycles (600 mA h g^{-1}, Fig. 7b). After 30 cycles, the same battery was further evaluated for rate capability as shown in Fig. 7c and d. When the current density is first increased from 0.2 C to 0.4 C, a stable high capacity of 927 mA h g^{-1} can still be achieved. Afterward, the rate is further increased stepwise up to 15 C. As an example, at a high rate of 3 C, these CoO@C nanohybrids can still deliver a stable capacity of about 483 mA h g^{-1} (Fig. 7d). Even at a high current density of 15 C, this material can still deliver a reversible capacity of 150 mA h g^{-1} (Fig. 7d). Remarkably, when the current rate is again reduced back to 0.2 C after more than 70 cycles, a stable high capacity of 990 mA h g^{-1} can be resumed (Fig. 7d). These electrochemical results suggest that the elastic porous nanostructured electrode has superior rate performances. During these whole charge/discharge cycles at different rates, the Coulombic efficiency steadily kept the values higher than 90% except for the first cycle (Fig. 7d). This performance is superior to

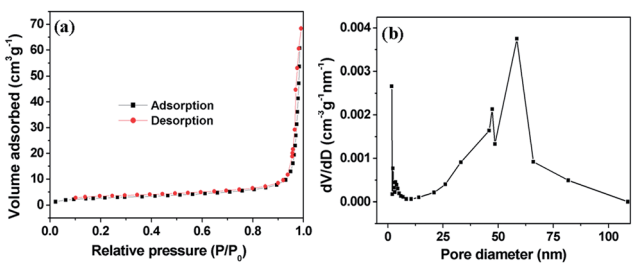

Fig. 6 N_2 adsorption/desorption isotherm and the corresponding pore size distribution of self-assembled porous hierarchical-like CoO@C microsheets calculated using BJH method.

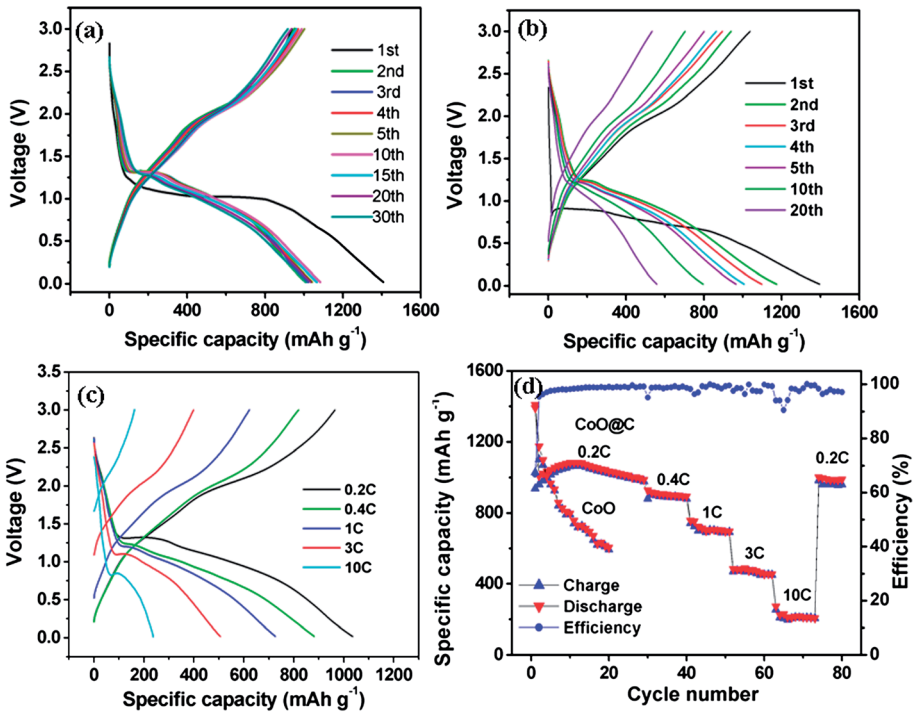

Fig. 7 Electrochemical performances CoO-based anodes: (a) charge/discharge profiles of self-assembled porous hierarchical-like CoO@C microsheets; (b) charge/discharge profiles of bare CoO microsheets; (c) contiguous charge/discharge profiles of porous hierarchical-like CoO@C microsheets at different rates; (d) cycling performance of porous hierarchical-like CoO@C microsheets at different rates, the cycling performance of bare CoO microsheets are also included.

some other cobalt oxide-based anodes,[16,19,20] such as our previously fabricated nanocapsules.[20] Besides, the current synthetic route for self-assembled porous nanocomposites is quite simple and low-cost, beneficial for the process scale-up.

The high reversible capacity of these hierarchical-like porous CoO@C microsheets can probably be attributed the distinct electrochemical activity of porous and hierarchical CoO microsheets and a synergetic effect of CoO and the thin carbon layer.[14,15] A schematic illustration of the Li^+ insertion/extraction mechanism for multi-layer CoO@C microsheets is shown in Fig. 8. Firstly, the uniform and continuous three-dimensional carbon thin layers between CoO porous nanosheets composed of tiny nanoparticle not only remarkably enhances the electrical conductivity (leading to the formation of thin solid electrolyte interface films on the electrode surface),[17] but also provides continuous conductive paths between CoO nanosheets and thus reduces the particle-to-particle interface resistance. Secondly, the void space between each pair of nanoparticles and nanosheets of the porous hierarchical CoO@C microsheets can easily be filled with the electrolyte, ensuring a high surface area being in contact with the electrolyte, and hence a large flux of Li ions across the interface. Both the carbon layer and the interspace provide elastic buffer spaces to accommodate the volume changes upon Li ion insertion/extraction.[31,32] Lastly, the extremely reduced particle dimension renders solid state diffusion of Li ions favourable. The above synergetic effect favors the large capacity as well as superior cycle performance of the porous interconnected CoO nanoparticle-based electrode.

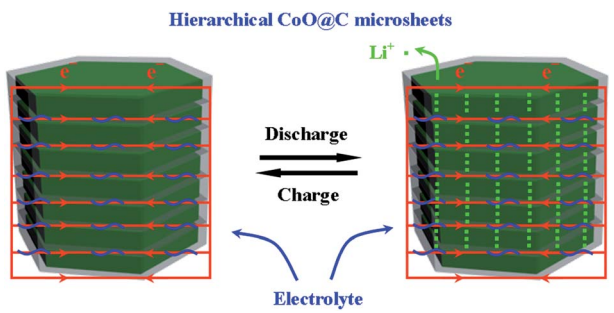

Fig. 8 Schematic illustration of Li^+ insertion/extraction process for porous hierarchical CoO@C microsheets.

4. Conclusion

We have successfully demonstrated the large-scale synthesis of self-assembled CoO@C hierarchical nanoarchitectures converted from inorganic–organic nanocomposites for lithium-ion battery application. The CoO interconnected nanoparticles are 20–60 nm in size and homogeneously distributed on two-dimensional thin carbon layers. Moreover, the flexible structure of two-dimensional carbon layers and the strong interaction between CoO nanoparticles and carbon layers in CoO@C nanocomposites are beneficial for efficiently preventing volume expansion/contraction and aggregation of CoO during Li charge/discharge process. Results show that these as-obtained hierarchical CoO@C nanocomposites exhibit highly reversible capacity (990 mA h g^{-1} after 30 cycles), excellent cyclability and good rate capability as anode materials in lithium-ion batteries.

The current inorganic–organic synergistic self-assembly method can be readily adopted to prepare other high-performance electrodes containing carbon materials as conducting additives that also bind lithium to further enhance capacity.

Acknowledgements

This work was financially supported by China Postdoctoral Science Foundation (2011M501279), Scientific Research Fund of Hunan Provincial Education Department (11C1198), the Key Special Project for Science and Technology of Hunan Province (2009FJ1002) and the Natural Science Foundation of Hunan Province for Innovation Group (09JJ7004).

References

1 M. Winter, J. O. Besenhard, M. E. Spahr and P. Novak, Insertion electrode materials for rechargeable lithium batteries, *Adv. Mater.*, 1998, **10**, 725–763.
2 B. Kang and G. Ceder, Battery materials for ultrafast charging and discharging, *Nature*, 2009, **458**, 190–193.
3 P. Poizot, S. Laruelle, S. Grugeon, L. Dupont and J. M. Tarascon, Nano-sized transition-metal oxides as negative-electrode materials for lithium-ion batteries, *Nature*, 2000, **407**, 496–499.
4 J. Liu and D. F. Xue, Hollow nanostructured anode materials for Li-ion batteries, *Nanoscale Res. Lett.*, 2010, **5**, 1525–1534.
5 J. Liu, H. Xia, D. F. Xue and L. Lu, Double-shelled nanocapsules of V_2O_5-based composites as high-performance anode and cathode materials for Li ion batteries, *J. Am. Chem. Soc.*, 2009, **131**, 12086–12087.
6 J. Liu, Y. C. Zhou, J. B. Wang, Y. Pan and D. F. Xue, Template-free solvothermal synthesis of yolk-shell V_2O_5 microspheres as cathode materials for Li-ion batteries, *Chem. Commun.*, 2011, **47**, 10380–10382.
7 J. Liu and D. F. Xue, Sn-based nanomaterials converted from SnS nanobelts: facile synthesis, characterizations, optical properties and energy storage performances, *Electrochim. Acta*, 2010, **56**, 243–250.
8 X. J. Zhu, Y. Zhu, S. Murali, M. D. Stoller and R. S. Ruoff, Nanostructured reduced graphene oxide/Fe_2O_3 composite as a high-performance anode material for lithium ion batteries, *ACS Nano*, 2011, **5**, 3333–3338.
9 M. Meruganandham, R. Amutha, M. Sathish, T. S. Singh, R. P. S. Suri and M. Sillanpaa, Facile fabrication of hierarchical α-Fe_2O_3: self-assembly and its magnetic and electrochemical properties, *J. Phys. Chem. C*, 2011, **115**, 18164–18173.
10 C. Ban, Z. Wu, D. T. Gillaspie, L. Chen, Y. Yan, J. L. Blackburn and A. C. Dillon, Nanostructured Fe_3O_4/SWNT electrode: binder-free and high-rate Li-ion anode, *Adv. Mater.*, 2010, **22**, E145–E149.
11 F. D. Wu and Y. Wang, Self-assembled echinus-like nanostructures of mesoporous CoO nanorod@CNT for lithium-ion batteries, *J. Mater. Chem.*, 2011, **21**, 6636–6641.
12 C. Yan, L. Nikolova, A. Dadvand, C. Harnagea, A. Sarkissian, D. F. Perepichka, D. F. Xue and F. Rosei, Multiple $NaNbO_3$/Nb_2O_5 heterostructure nanotubes: a new class of ferroelectric/semiconductor nanomaterials, *Adv. Mater.*, 2010, **22**, 1741–1745.
13 J. Hassoun, G. Derrien, S. Panero and B. A. Scrosati, Nanostructured Sn–C composite lithium battery electrode with unique stability and high electrochemical performance, *Adv. Mater.*, 2008, **20**, 3169–3175.
14 X. Xue, Z. Chen, L. Xing, S. Yuan and Y. Chen, SnO_2/α-MoO_3 core-shell nanobelts and their extraordinarily high reversible capacity as lithium-ion battery anodes, *Chem. Commun.*, 2011, **47**, 5205–5207.
15 F. Lu, Y. C. Zhou, J. Liu and Y. Pan, Enhancement of F-doping on the electrochemical behavior of carbon-coated $LiFePO_4$ nanoparticles prepared by hydrothermal route, *Electrochim. Acta*, 2011, **56**, 8833–8838.
16 L. Zhi, Y. S. Hu, B. E. Hamaoui, X. Wang, I. Lieberwirth, U. Kolb, J. Maier and K. Müllen, Precursor-controlled formation of novel carbon/metal and carbon/metal oxide nanocomposites, *Adv. Mater.*, 2008, **20**, 1728–1731.
17 F. Cao, D. Wang, R. Deng, J. Tang, S. Song, Y. Lei, S. Wang, S. Su, X. Yang and H. Zhang, Porous Co_3O_4 microcubes: hydrothermal synthesis, catalytic and magnetic properties, *CrystEngComm*, 2011, **13**, 2123–2129.
18 D. Barreca, A. Gasparotto, O. I. Lebedev, C. Maccato, A. Pozza, E. Tondello, S. Turner and G. Van Tendeloo, Controlled-vapor-phase synthesis of cobalt oxide nanomaterials with tuned composition and spatial organization, *CrystEngComm*, 2010, **12**, 2185–2197.
19 J. Ryu, S. W. Kim, K. Kang and C. B. Park, Synthesis of diphenylalanine/cobalt oxide hybrid nanowires and their application to energy storage, *ACS Nano*, 2010, **4**, 159–164.
20 J. Liu, H. Xia, L. Lu and D. F. Xue, Anisotropic Co_3O_4 porous nanocapsules toward high-capacity Li-ion batteries, *J. Mater. Chem.*, 2010, **20**, 1506–1510.
21 Y. Li, B. Tan and Y. Wu, Mesoporous Co_3O_4 nanowire arrays for lithium ion batteries with high capacity and rate capability, *Nano Lett.*, 2008, **8**, 265–270.
22 X. W. Lou, D. Deng, J. Y. Lee, J. Feng and L. A. Archer, Self-supported formation of needlelike Co_3O_4 nanotubes and their application as lithium-ion battery electrodes, *Adv. Mater.*, 2008, **20**, 252–262.
23 J. Liu, F. Liu, K. Gao, J. S. Wu and D. F. Xue, Recent developments in the chemical synthesis of inorganic porous capsules, *J. Mater. Chem.*, 2009, **19**, 6073–6084.
24 J. W. Lee, J. M. Ko and J. D. Kim, Hierarchical microspheres based on α-$Ni(OH)_2$ nanosheets intercalated with different anions: synthesis, anion exchange, and effect of intercalated anions on electrochemical capacitance, *J. Phys. Chem. C*, 2011, **115**, 19445–19454.
25 M. Taibi, S. Ammar, N. Jouini, F. Fievet, P. Molinie and M. Drillon, Layered nickel hydroxide salts: synthesis, characterization and magnetic behaviour in relation to the basal spacing, *J. Mater. Chem.*, 2002, **12**, 3238–3244.
26 N. Ikawa, Y. Oumi, T. Kimura, T. Ikeda and T. Sano, Synthesis of lamellar mesostructured calcium phosphates using *n*-alkylamines as structure-directing agents in alcohol/water mixed solvent systems, *J. Mater. Sci.*, 2008, **43**, 4198–4207.
27 M. Y. Cheng and B. J. Hwang, Control of uniform nanostructured α-$Ni(OH)_2$ with self-assembly sodium dodecyl sulfate template, *J. Colloid Interface Sci.*, 2009, **337**, 265–271.
28 A. Clearfield, M. Kieke, J. Kwan, J. L. Colon and R. C. Wang, Intercalation of organic and inorganic anions into layered double hydroxides, *J. Inclusion Phenom. Mol. Recognit. Chem.*, 1991, **11**, 361–378.
29 R. S. Jayashree and P. V. Kamath, Electrochemical synthesis of α-cobalt hydroxide, *J. Mater. Chem.*, 1999, **9**, 961–963.
30 J. M. Wu and Y. R. Chen, Ultraviolet-light-assisted formation of ZnO nanowires in ambient air: comparison of photoresponsive and photocatalytic activities in zinc hydroxide, *J. Phys. Chem. C*, 2011, **115**, 2235–2243.
31 D. Wang, R. Kou, D. Choi, Z. Yang, Z. Nie, J. Li, L. V. Saraf, D. Hu, J. Zhang, G. L. Graff, J. Liu, M. A. Pope and I. A. Aksay, Ternary self-assembly of ordered metal oxide–graphene nanocomposites for electrochemical energy storage, *ACS Nano*, 2010, **4**, 1587–1595.
32 H. X. Zhang, C. Feng, Y. C. Zhai, K. L. Jiang, Q. Q. Li and S. S. Fan, Cross-stacked carbon nanotube sheets uniformly loaded with SnO_2 nanoparticles: a novel binder-free and high-capacity anode material for lithium-ion batteries, *Adv. Mater.*, 2009, **21**, 2299–2304.

